

PAPER

Low lattice thermal conductivity and excellent thermoelectric behavior in Li_3Sb and Li_3Bi

To cite this article: Xiuxian Yang *et al* 2018 *J. Phys.: Condens. Matter* **30** 425401

View the [article online](#) for updates and enhancements.




IOP | ebooks™

Bringing you innovative digital publishing with leading voices to create your essential collection of books in STEM research.

Start exploring the **collection** - download the first chapter of every title for free.

Low lattice thermal conductivity and excellent thermoelectric behavior in Li_3Sb and Li_3Bi

Xiuxian Yang¹, Zhenhong Dai^{1,3} , Yinchang Zhao^{1,3}, Jianye Liu¹ and Sheng Meng^{2,3}

¹ Department of Physics, Yantai University, Yantai 264005, People's Republic of China

² Beijing National Laboratory for Condensed Matter Physics and Institute of Physics, Chinese Academy of Sciences, Beijing 100190, People's Republic of China

E-mail: zh dai@ytu.edu.cn, y.zhao@ytu.edu.cn and smeng@iphy.ac.cn

Received 20 June 2018, revised 29 August 2018

Accepted for publication 31 August 2018

Published 3 October 2018



Abstract

Utilizing the first-principle calculations combined with Boltzmann transport equation and semiclassical analysis, we present a systematic investigation of the electron structure, lattice thermal conductivity κ_L , Seebeck coefficient S , and the dimensionless figure of merit ZT of crystal Li_3Sb and Li_3Bi . The κ_L of 2.2 and 2.09 W m⁻¹ K⁻¹ are obtained at room temperature in Li_3Sb and Li_3Bi systems with the band gap of 0.68, 0.34 eV, respectively. The low κ_L can induce excellent thermoelectric properties. Thus the effect of doping on the transport properties has been judiciously researched and the maximum ZT of 2.42, 1.54 is obtained at 900 K in the p-type doped Li_3Sb and p-type doped Li_3Bi with the stable structures. Up to date, experimental finding of the maximum ZT is 2.6 at 850 K in the Cu_2Se sample with 1 mol indium, our results are very close to this value. This letter provides insight into the thermal transport properties of Li_3Sb and Li_3Bi , meanwhile, supports that crystalline Li_3Sb and Li_3Bi may be promising materials for thermoelectric devices and application.

Keywords: thermoelectric property, first-principle, lattice thermal dynamics, thermal transport

(Some figures may appear in colour only in the online journal)

1. Introduction

The thermoelectric (TE) materials provide a clean way to utilize the waste heat from the transportation applications or the high-temperature industrial and directly change heat to electricity, which have attracted a large interests in the recent decades [1–3]. However, the prime obstruction in replacing the traditional power generation is the low conversion efficiency in TE materials [4, 5]. The dimensionless figure of merit $ZT = \sigma S^2 T / \kappa$ is a primary measure of TE materials performance, which defines the conversion efficiency of TE materials, where σ is the electrical conductivity, S is the Seebeck coefficient, T is the absolute temperature and κ is the thermal conductivity. κ can write as $\kappa = \kappa_e + \kappa_L$, where κ_e represents

thermal conductivity from electrons and κ_L from the lattice. Therefore, investigating both electron and lattice thermal transport properties can reveal complete TE performances. In addition, the power factor σS^2 is also used to estimate the TE features. Thus, enhancing ZT or σS^2 requires optimizing the adversely interdependent σ , S and κ as a group [1, 6].

For enhancing the ZT or σS^2 , there have been a lot of strategies proposed. For instance, in p-type PbTe, a distortion of the electronic density of states by the resonant impurities (Ti) can induce a drastic improvement S , hence a high ZT of 1.5 was achieved at 773 K [7, 8]. Due to the conduction band convergence, it can lead to a significantly enhanced S with no adverse effect on the carrier mobility in $\text{Mg}_2\text{Si}_{1-x}\text{Sn}_x$ solid solutions, hence a maximum value of $ZT \sim 1.3$ was obtained at 700 K in this composite material [9]. In solution-processed Sb_2Te_3 with inserted silver nano-particles as the non-planar

³ Authors to whom any correspondence should be addressed.

barriers, ZT and σS^2 were enhanced drastically due to the carrier energy filtering effect [10, 11]. In addition, besides these methods for improving the TE properties, the reduction of κ_L is also a commonly strategy in the nano-structured materials, which have caused significant enhancements of ZT by increased phonon scattering around the grain boundaries, structure defects, and interfaces [12, 13]. For example, an enormous ZT value of 2.6 was obtained at 850 K in the Cu_2Se with 1 mol% indium, which is attributed to the localization of Cu^+ induced by the incorporation of indium into the Cu_2Se lattice and simultaneously boosting the electrical conductivity and reducing the thermal conductivity of the nanocomposites [14]. In skutterudites CoSb_3 , by filling Ba atom the calculated κ_L has dropped significantly [15]. In addition, there are many other materials with low κ_L and good TE properties, such as PbTiO_3 , CdO [16], fully filled skutterudite YbFe_4Sb_3 [17], n-type TiO_2 polymorphs [18], nanoporous bulk silicon [19], etc. Most of materials contain the heavier atoms from the perspective of composition, which are beneficial for increasing the intrinsic phonon scattering and thus reducing the κ_L [3].

Therefore, for TE applications the ideal materials have both low κ_L and high σS^2 . Lithium materials have been used to make lithium batteries [20–22]. However, recent experiments have found that doping lithium enhances the TE performance of MgAgSb [23] and theory calculations have found that LiH and NaH have higher ZT values [3, 24]. Thus, we take the lithium-based semiconductor materials (Li_3Sb and Li_3Bi) containing heavier atoms (Sb, Bi) as an example to systematically investigate the heat and electronic transport properties, and we conclude that these materials have low κ_L , high σS^2 and hence excellent thermoelectric behaviors. The paper is organized as follows. We briefly introduce the theoretical methods in section 2. The results on our calculations are presented in section 3. In section 4 is a summary of our work.

2. Methodology

Firstly, we study the κ_L of these materials via solving the phonon Boltzmann transport equation (BTE) using relaxation times approximation (RTA) method with interatomic forces from density functional theory (DFT) [25]. For the cubic crystal structures, the κ_L is a scalar quantity and given by

$$\kappa_L^{\alpha\alpha} = \frac{1}{NV} \sum_{\lambda} \frac{\partial f_{\lambda}}{\partial T} (\hbar\omega_{\lambda}) \nu_{\lambda}^{\alpha} \nu_{\lambda}^{\alpha} \tau, \quad (1)$$

where N is the number of quasi continuous q points uniformly sampled in the first Brillouin zone (BZ), V is the unit cell volume, T is absolute temperature. λ is phonon mode, which consists of both the phonon branch p and wave vector \mathbf{q} . f_{λ} is the equilibrium Bose–Einstein distribution function, which depends on the phonon frequency ω_{λ} , respectively. \hbar is the reduced Planck constant, and ν_{λ}^{α} is the phonon group velocity of mode λ along α direction. τ is phonon relaxation times in phonon RTA.

The first-principle calculations were carried out within the DFT frame as employed in the Vienna *Ab initio* Simulation Package (VASP) [26, 27]. The ions cores were modeled by

the projector augmented wave potentials (PAW) [28], while the valance electrons were described by a plane-wave basis set with the cutoff energy of 550 eV and the exchange-correlation functional of the generalized gradient approximation of the Perdew–Burke–Ernzerhof [29] is used. The electronic stopping criterion is set to 10^{-8} eV and the force criteria for ions is 10^{-8} eV. We use a $20 \times 20 \times 20$ Γ -centered Monkhorst–Pack k -points mesh to simulate the Brillouin zone integration in relaxation process. The ShengBTE [25] package is used to calculate the κ_L with $20 \times 20 \times 20$ q -mesh. The harmonic (second-order) and anharmonic (third-order) interatomic force constants (IFCs) required in ShengBTE calculations are computed by VASP combined with PHONOPY program [27] and the thirdorder.py script [25], respectively. The harmonic IFCs was calculated using $4 \times 4 \times 4$ supercells and $5 \times 5 \times 5$ k -points by finite-difference approach in PHONOPY program. The anharmonic IFCs was obtained using $4 \times 4 \times 4$ supercells and Γ -point-only calculations via finite-difference approach in the thirdorder.py script. In our calculations, the interactions were considered out to four-nearest neighbors of the unit-cell atoms for anharmonic IFCs.

To obtain the electron transport properties, we calculate the S , κ_{el} , and σ using the rigid-band approach and the semiclassical Boltzmann theory, which is performed in the BOLTZTRAP code [30] and utilizing the constant scattering time approximation. In this method, the electron scattering time τ_e is the only empirical parameter, which can determine the σ and κ_{el} . Experimental results on mobility, carrier concentration, and σ can be used to estimate τ_e . In our calculations, the values of τ varies between 1 and 9 fs. The electronic structure is recalculated by VASP on the dense k -points of $55 \times 55 \times 55$ to acquire derivatives of the Kohn–Sham eigenvalues. At all calculations, we use the fully relax crystal structures with the optimized lattice parameters and the results ensured convergence.

3. Results and discussion

Figure 1(a) gives the crystal structure of α - Li_3Sb (For simplicity, in the following α - Li_3Sb also called Li_3Sb if no special instructions.) and Li_3Bi unit cell. They have a face centered cubic structure with the $\text{Fm}\bar{3}\text{m}$ (No. 225) space group and four atoms in the primitive cell. The optimized lattice constants are 6.56 Å and 6.74 Å for Li_3Sb and Li_3Bi , respectively, which are well agreement with the other experimental and theoretical results [31–35]. Red and blue spheres represent Li and Bi (or Sb) atoms. The length of Li–Sb and Li–Bi bond in crystal structure are 2.84 Å and 2.92 Å, respectively. In addition, the calculated energy band and total electron density of states (DOS) of these materials are plotted in figure 1(b). Li_3Sb and Li_3Bi are narrow band gap semiconductors with the band gap of 0.68 eV and 0.34 eV, respectively, which are consistent with other works [35]. Through comparing, one can see that the energy bands have same trend and the conduction band minima (CBM) state is located at the high-symmetry X point, the valence band maxima (VBM) state is located along the K- Γ line, which indicates that these materials are indirect band gap semiconductors. Due to the similar band structure,

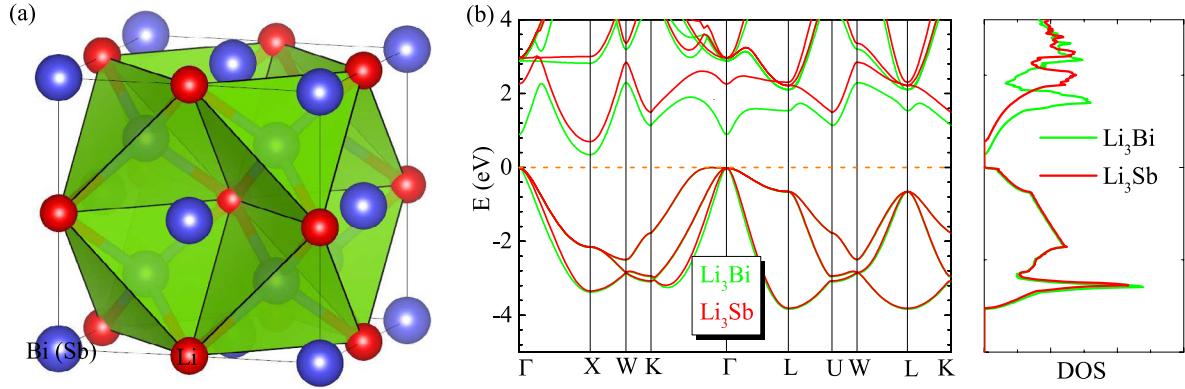


Figure 1. (a) Crystal structure of Li_3Bi or Li_3Sb (space group of $\text{Fm}\bar{3}\text{m}$) unit cell. Red and blue spheres represent Li and Bi (or Sb) atoms. (b) Electron bands and total electron density of states (DOS) of Li_3Bi (green curves) and Li_3Sb (red curves) along the high symmetry point within the first Brillouin zone (BZ), respectively.

the total DOS of Li_3Sb and Li_3Bi have same trend as well. It should be noted that a small platform is near the Fermi level, indicating a large electronic effective mass, which may help to obtain large Seebeck coefficient. The band effective mass is given by

$$m^* = \hbar^2 / \frac{\partial^2 E}{\partial k^2}, \quad (2)$$

where m^* is band effective mass. For electron (hole), $m^* = m_n^*$ (m_p^*). The electronic density of state (EDOS) effective masses were calculated approximated by the equation of

$$g_c(E) = \frac{V}{2\pi^2} \frac{(2m_{dn}^*)^{3/2}}{\hbar^3} (E - E_c)^{1/2}, \quad (3)$$

and

$$g_v(E) = \frac{V}{2\pi^2} \frac{(2m_{dp}^*)^{3/2}}{\hbar^3} (E_v - E)^{1/2}, \quad (4)$$

where $g_c(E)$ is EDOS near the conduction band minima (CBM) and the valence band maxima (VBM), V is the volume of primitive cell, \hbar is reduced Planck constant. m_{dn}^* (or m_{dp}^*) is EDOS effective mass of electron (hole), E_c (or E_v) is the energy level of CBM (or VBM), respectively. For Li_3Sb , m_n^* are 0.602 and $0.294m_0$ along X- Γ and X-W path, m_p^* are 3.234 and $1.345m_0$ along VBM- Γ and VBM-K path, respectively, meanwhile m_{dn}^* is $3.840m_0$ and m_{dp}^* is $8.675m_0$. For Li_3Bi , m_n^* are 0.554 and $0.283m_0$ along X- Γ and X-W path, m_p^* are 3.340 and $1.160m_0$ along VBM- Γ and VBM-K path, respectively, also m_{dn}^* is $3.420m_0$ and m_{dp}^* is $8.500m_0$.

The calculated phonon dispersions and partial phonon density of states (PDOS) of Li_3Sb (a) and Li_3Bi (b) are presented by the red curves in figure 2, respectively. One can see that the amplitude of phonon frequencies of Li_3Sb are larger than that of Li_3Bi , while a phonon gap between acoustic phonon modes and optic phonon modes of about 0.63 THz for Li_3Sb is smaller than that of 1.62 THz for Li_3Bi . We consider that this is because of the change of mass ratio of the constituent atoms. To confirm our guess, we artificially change the atom mass of Sb to that of Bi and the results are presented by the green curves in figure 2(b) compared to Li_3Bi (the red curves). The phonon gap can be expanded and the amplitude

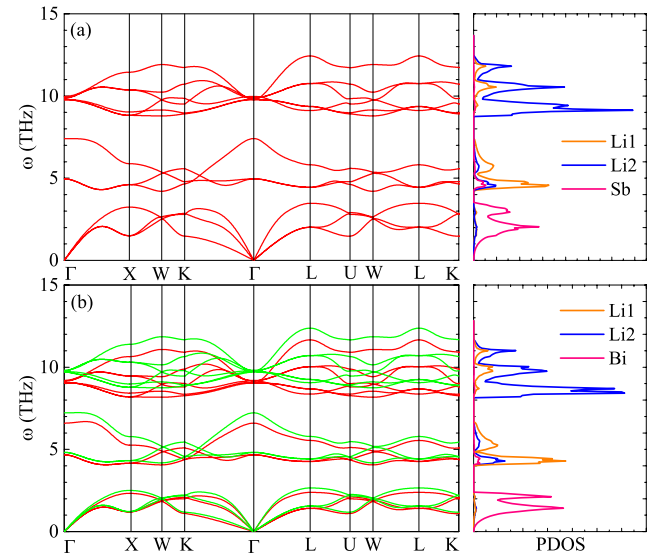


Figure 2. Calculating phonon dispersion relations and partial phonon density of states (PDOS) of Li_3Sb (a) and Li_3Bi (b) along the high symmetry point within the first Brillouin zone (BZ), respectively. In figure (b) the green curves represent the Li_3Sb with the mass of Sb atom replaced by that of Bi atom. Due a similar crystal structure, the PDOS of each system exhibits analogous behaviors.

of acoustic phonon frequencies can be decreased due to the change of atom mass. In addition, by this way we obtained the acoustic phonon modes matching well those for Li_3Bi , which indicates that the change of low frequency acoustic phonon modes and phonon gap are almost entire due to the atom mass increasing from Sb to Bi. The calculated partial PDOS for these materials are presented in figure 2, and it shows that almost all of the optic phonon modes are afforded by the light atoms (Li atom) and the acoustic phonon modes are afforded by the heavier atom (Sb or Bi atom for different materials). It is found that three Li atoms in a unit cell can be divided into two groups: Li1 only contains one Li atom and Li2 contains two Li atoms. Utilizing the phonon spectrum can inspect the structure stability and the crystal structure stability lies in the fact that for each phonon mode the frequency should be a real quantity and not imaginary [36, 37]. For these materials there

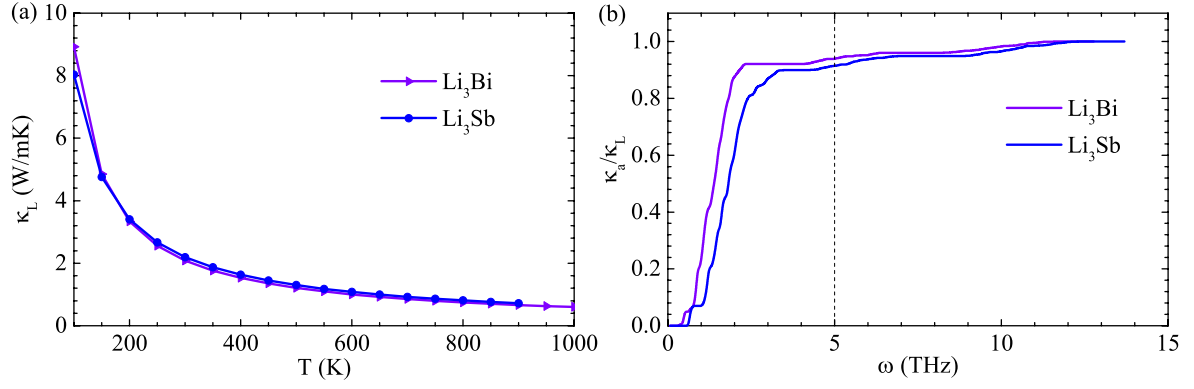


Figure 3. (a) Lattice thermal conductivity κ_L for Li_3Sb (blue circles) and Li_3Bi (violet triangles). Since the α - Li_3Sb transforms to β - Li_3Sb when temperature exceeds 923 K, we only give the κ_L at 100–900 K. (b) The accumulative lattice thermal conductivity κ_a scaled by the total κ_L of Li_3Sb (blue line) and Li_3Bi (violet line) as a function of frequency at the room temperature, respectively.

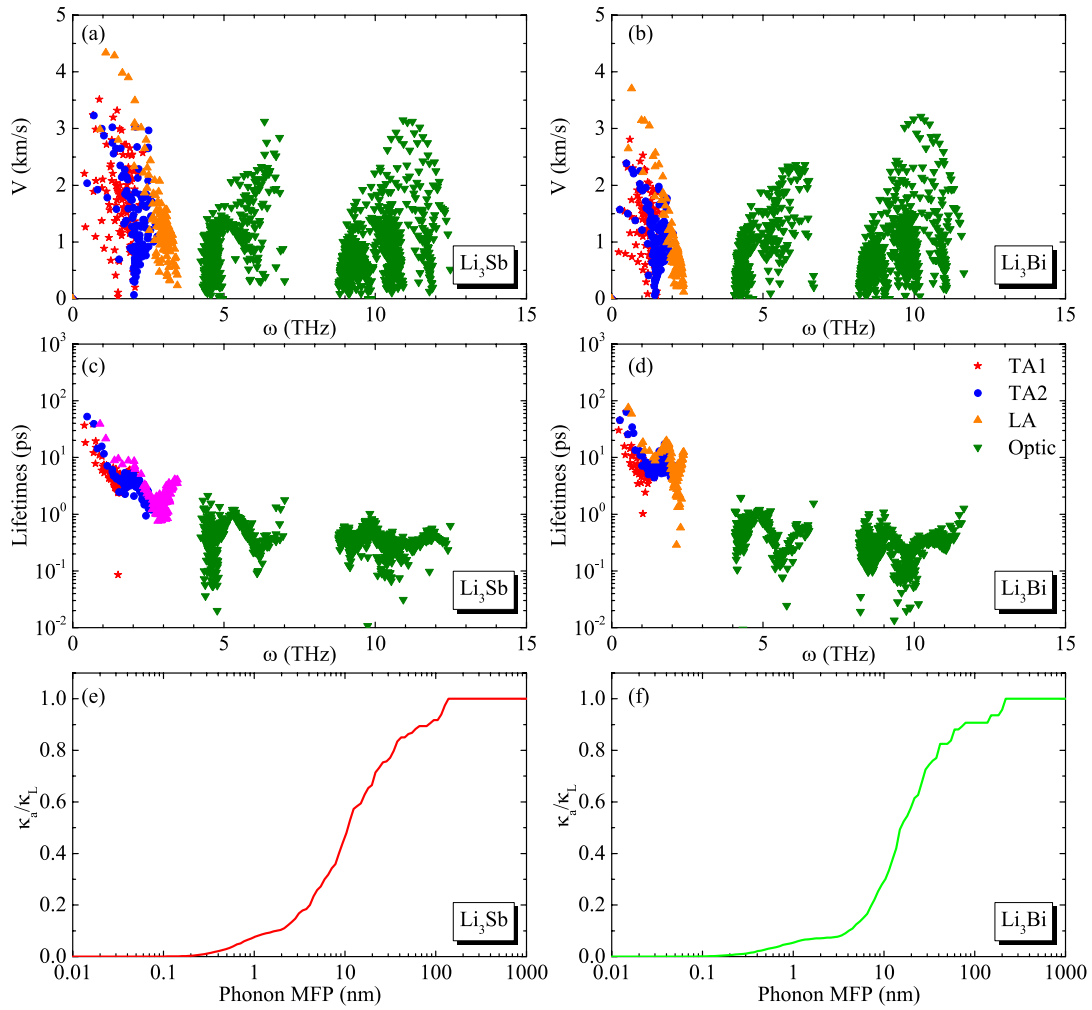


Figure 4. Phonon group velocities ((a) and (b)) and lifetimes ((c) and (d)) of all phonon modes as a function of frequency for Li_3Sb and Li_3Bi at 300 K, respectively. In (a)–(d), the red pentagrams, blue circles, orange upper triangles and green lower triangles represent the TA1, TA2, LA and optic modes, respectively. (e) and (f) The cumulative thermal conductivity κ_a scaled by the κ_L versus phonon maximum mean-free path (MFP) for Li_3Sb and Li_3Bi at 300 K.

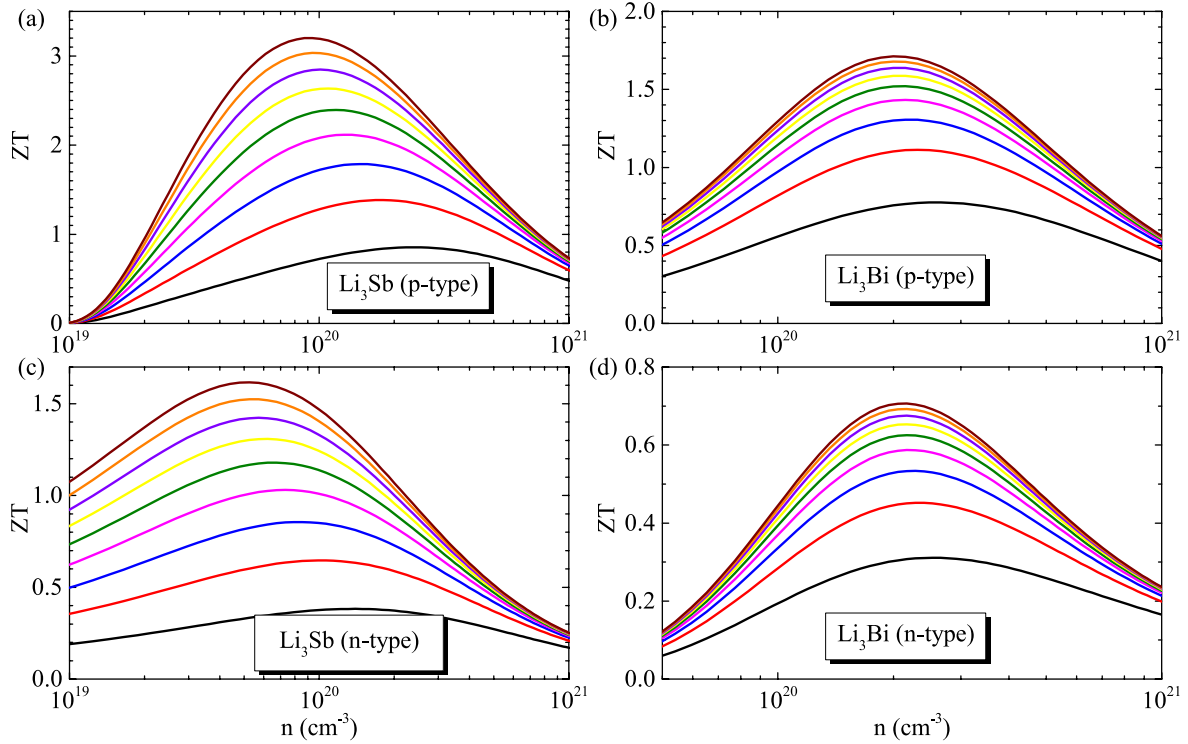


Figure 5. The trend of ZT at 900 K for Li_3Sb and Li_3Bi as a function of carriers concentration (n), respectively. The (a) and (b) are p-type doped and ((c) and (d)) are n-type doped for these materials. The black, red, blue, pink, green, yellow, violet, orange and wine solid curves represent the values with $\tau = 1, 2, 3, 4, 5, 6, 7, 8, 9$, respectively.

are no imaginary frequencies, thus we can ensure the dynamic stability of Li_3Sb and Li_3Bi . In addition, the Debye temperature Θ_D was calculated by the equation of

$$\Theta_D = \frac{h\nu_m}{k_B}, \quad (5)$$

where k_B is the Boltzmann constant, h is Planck constant, ν_m is the highest frequency of normal mode vibration. For Li_3Sb and Li_3Bi , the values of ν_m are 3.56 and 2.38 THz, thus the calculated Θ_D are 171.03 and 114.34 K, respectively.

Figure 3(a) gives the lattice thermal conductivity κ_L versus temperature for Li_3Sb (blue circles) and Li_3Bi (violet triangles). Since the α - Li_3Sb transforms to β - Li_3Sb when temperature exceeds 923 K [31], we only give the κ_L in the range of 100–900 K for α - Li_3Sb . The Li_3Bi can remain initial structure up to 1438 ± 40 K [32], thus the κ_L in the temperature range of 100–1000 K were given. The low κ_L of 2.2 and 2.09 $\text{W m}^{-1} \text{K}^{-1}$ are obtained in Li_3Sb and Li_3Bi crystal structure at the room temperature, which are much smaller than CoSb_3 (11.5 $\text{W m}^{-1} \text{K}^{-1}$) [15], n-type half-Heusler materials $\text{Hf}_{0.75}\text{Zr}_{0.25}\text{NiSn}_{0.99}\text{Sb}_{0.01}$ (4.0–4.6 $\text{W m}^{-1} \text{K}^{-1}$) [38], p-type silicon germanium bulk alloys (2.4–2.8 $\text{W m}^{-1} \text{K}^{-1}$) [39], etc. In addition, to gain more insight into the κ_L of these materials, we also examine which phonon modes provide the dominant thermal conductivity. Figure 3(b) gives the accumulative lattice thermal conductivity κ_a as a function of frequency, and for clarity scaled by the total κ_L for Li_3Sb (blue line) and Li_3Bi (violet line) at the room temperature. κ_a gives the summed contribution from all phonon modes below the specified frequency. For Li_3Bi phonons with frequency below 5 THz

transport more than 92% of the heat, while for Li_3Sb this is a bit less. Additionally, three acoustic phonon modes dominate the heat transport in these materials. Therefore, by doping other atoms or other methods to engender more phonon scattering channels between the acoustic phonon modes and optic phonon modes, the κ_L would further decrease. Nevertheless, this is not the key point in our work.

To gain further insights into the thermal transport mechanism, the phonon group velocities (a) and (b) and phonon lifetimes (c) and (d) of all phonon modes as a function of frequency are given in figure 4 for Li_3Sb and Li_3Bi at 300 K, respectively. From figures 2 and 3(b), there are 12 phonon modes, while three acoustic phonon modes dominate the heat transport in these materials. Therefore, we restrict our subsequent discussions to the transverse mode (TA1), the transverse mode (TA2) and the longitudinal mode (LA), which is denoted by the red pentagrams, blue circles, orange upper triangles. Other optic modes are denoted by green lower triangles. The phonon group velocities are determined by the phonon frequency. With the heavier atomic mass, Li_3Bi has much lower group velocities than Li_3Sb , as shown in figures 4(a) and (b). For the TA and LA modes, the maximum group velocities of Li_3Bi are about 2.81 and 3.70 km s^{-1} , respectively, while those of Li_3Sb are about 3.51 and 4.36 km s^{-1} , respectively. Phonon scattering is a key feature to reveal the thermal transport mechanism. Larger phonon scattering rate gives smaller phonon lifetimes. Figures 4(c) and (d) show the lifetimes of all phonon modes. One can find that Li_3Sb has smaller phonon lifetimes than Li_3Bi , which hints that Li_3Sb has stronger phonon scattering. The lower κ_L

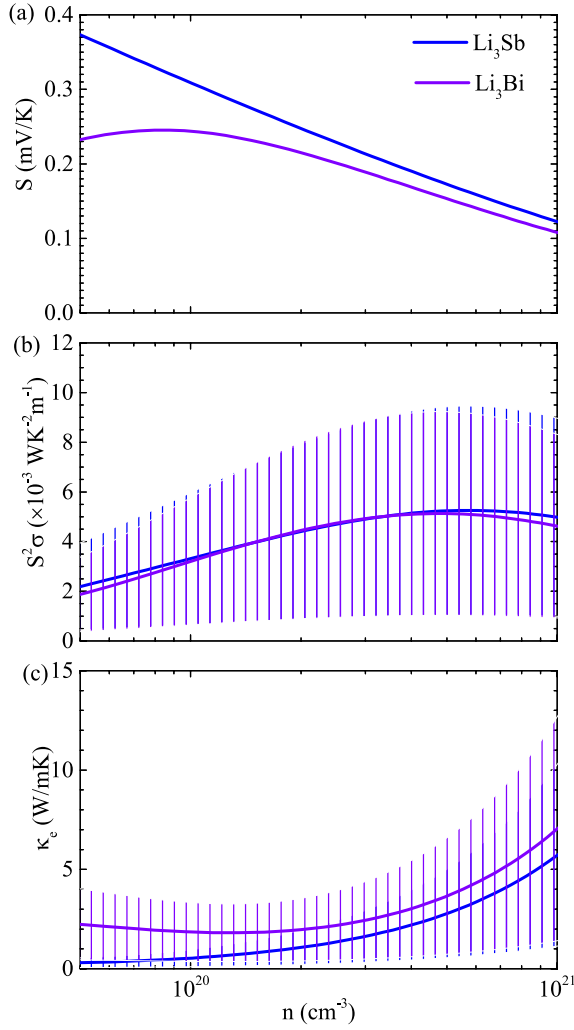


Figure 6. The TE parameters as a function of carriers concentration (n) for p-type doped Li₃Sb (blue curves) and p-type doped Li₃Bi (violet curves) at 900 K. (a) Thermopower S . (b) Power factor $S^2\sigma$. (c) Electronic thermal conductivity κ_e . In ((b) and (c)), the upper and lower limits of the vertical bars and the full curves represent the values with $\tau = 9, 1$, and 5 fs.

in Li₃Bi indicates that phonon group velocities have a more important role in the heat transport than phonon scattering for these materials. Figures 4(e) and (f) describes the contribution from phonon with the allowed phonon maximum mean-free path (MFP) at 300 K. The cumulative thermal conductivity κ_a is normalized to the κ_L . It can be seen that the κ_a value keeps increasing as the MFP increases, until reaching the thermodynamic limit, which represents the thermal carries for the longest phonon MFP and possesses values of 138.95 and 220.09 nm for Li₃Sb and Li₃Bi. Nanostructuring with the characteristic length smaller than 10 nm can reduce the total κ_L by 53.1% and 70.2% for Li₃Sb and Li₃Bi.

Due to the low κ_L for these materials, it is worth to investigate their TE performances. Figure 5 illustrates the dimensionless figure of merit ZT at 900 K. Figures 5(a) and (b) are p-type doped Li₃Sb and Li₃Bi, (c) and (d) are n-type doped Li₃Sb and Li₃Bi, respectively. To consider the effect of electronic scattering times τ , a simple formula $\tau \sim d/v$ is used to roughly

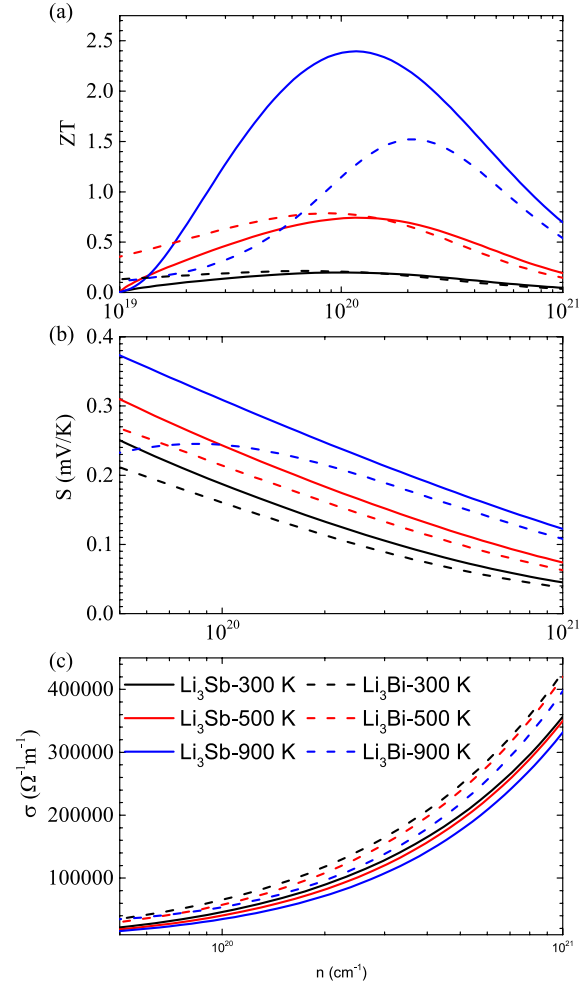


Figure 7. The TE parameters as a function of carriers concentration (n) for p-type doped Li₃Sb (solid lines) and Li₃Bi (dash lines) at 300, 500 and 900 K. (a) ZT. (b) Thermopower S . (c) Electrical conductivity σ . The black, red, and blue curves represent the temperature with 300, 500 and 900 K, respectively. Here, electronic scattering times is 5 fs.

estimate the amplitude of electronic scattering time τ , where d is the average electron–electron distance, which is estimated by the doping concentration. v is electron velocity, which is estimated by formula $v = \frac{1}{\hbar} \frac{\partial E}{\partial k}$. In our work, the doping concentration is 10²⁰ cm⁻³ and $v \approx 8 \times 10^5$ m s⁻¹, thus τ is about the order of magnitude of dozens of femtoseconds (fs). Considering the effect of lattice vibration, impurity scattering and other scattering mechanism, the value of τ from 1 to 9 fs was used. Our results show that at 900 K ZT often exceeds 1 as electronic scattering time τ varies between 1 and 9 fs in p-type doped Li₃Sb (figure 5(a)). Besides the p-type doping, the cases with n-type doped Li₃Sb (figure 5(c)) also exhibit good TE performances. ZT also exceeds 1 as τ varies between 1 and 9 fs. The fairly large ZT value is 2.42 (1.20) with $\tau = 5$ fs at 900 K and $n \approx 1.8 \times 10^{20}$ cm⁻³ ($n \approx 6.5 \times 10^{19}$ cm⁻³) in p-type (n-type) doped Li₃Sb, respectively. The extraordinarily high ZT is 3.21 and 1.62 as τ increases to 9 fs at $n \approx 9.6 \times 10^{19}$ cm⁻³ and $n \approx 5.57 \times 10^{19}$ cm⁻³ in p-type doped and n-type Li₃Sb, while the maximum ZT of 0.87 and 0.39 are obtained at higher carriers concentration if τ is lower

to only 1 fs. However, the TE performance of Li_3Bi is not good compared with Li_3Sb . For example, the maximum ZT of 1.54 and 1.72 are obtained at 900 K with $\tau = 5$ and 9 fs in p-type Li_3Bi , as shown in figure 5(b), respectively. The case of n-type doped Li_3Bi shows more bad TE performance, such as the maximum ZT of 0.71 with $\tau = 9$ fs. These results suggest that Li_3Sb is a good TE materials than Li_3Bi , and the cases of p-type doping have better TE performance than n-type doping for these materials. The ZT of p-type doped Li_3Sb is higher than the current commercial TE materials, such as PbTe (ZT 2.2) [40] and other advanced TE materials like $\text{Yb}_x\text{Co}_4\text{Sb}_{12}$ ($zT \sim 1.2$) [41], and NbFeSb -based p-type half-Heuslers ($zT \sim 1$) [42]. Up to date, an unprecedentedly large value of 2.6 at 850 K was obtained in Cu_2Se with 1 mol indium sample [14] and our calculation results are very close to this value. In addition, the ZT values with $\tau = 5$ fs at 300, 500 and 900 K were plotted in figure 7(a). For these materials, the ZT values keep increasing as the temperature increases and the ZT values exceed 0.7 (0.2) when temperature is 500 (300) K.

There is a large difference of ZT between Li_3Sb and Li_3Bi , although κ_L of Li_3Bi is slightly smaller than that of Li_3Sb . To explain this phenomenon, we examine the TE parameters such as Seebeck coefficient S , power factor $S^2\sigma$ and electrical thermal conductivity κ_e of Li_3Sb (blue curves) and Li_3Bi (violet curves), as shown in figure 6. These parameters are calculated by the BOLTZTRAP code [30] and we only consider p-type doping because the maximum ZT is obtained in these materials with the p-type doping. From figure 6(a), one can see that Seebeck coefficient S for Li_3Sb is larger than that of Li_3Bi in the same carrier concentration range of 5×10^{19} – 10^{21} cm^{-3} . Additionally, figure 7(b) shows that S for Li_3Sb is larger than that of Li_3Bi at same temperature. However, the power factor $S^2\sigma$ (figure 5(b)) has no significantly difference, thus concluding that σ of Li_3Bi is larger than that of Li_3Sb , as shown in figure 7(c). In addition, it is necessarily to calculate κ_e , although it is smaller compared to κ_L in semiconductor materials. Figure 6(c) shows Li_3Sb has smaller κ_e . These results explain why Li_3Sb has a higher ZT compared to Li_3Bi by the formula $ZT = S^2\sigma T / (\kappa_L + \kappa_e)$, thus a excellent TE performance.

4. Conclusion

To summarize, we have studied the electronic structure and thermal transport properties of Li_3Sb and Li_3Bi from the first principle calculations together with the Boltzmann transport theory. These materials are narrow band gap semiconductor (0.68 eV for Li_3Sb and 0.34 eV for Li_3Bi) and have low κ_L ($2.2 \text{ W m}^{-1} \text{ K}^{-1}$ for Li_3Sb and $2.09 \text{ W m}^{-1} \text{ K}^{-1}$ for Li_3Bi at the room temperature). In addition, the role of atomic mass in the phonon spectrum is studied and the results show that acoustic phonon modes mainly arise from the shake of heavier atom (Sb or Bi atom). Considering the low κ_L , it is necessary to study the TE properties of these materials. Therefore, we have used a combination of the first principle calculations and the semiclassical analysis to investigate the dimensionless figure of merit ZT of these materials. As a result, the higher ZT of these materials is obtained in Li_3Sb and Li_3Bi . As the

τ varies between 1 fs and 9 fs, the ZT values often exceed 1. Remarkably, the high ZT of 2.42 and 1.20 are achieved in p-type doped and n-type doped Li_3Sb with $\tau = 5$ fs. Besides, ZT of 1.54 is obtained in p-type doped Li_3Bi at 900 K with $\tau = 5$ fs. The superhigh ZT of 3.21 is obtained in p-type doped Li_3Sb with $\tau = 9$ fs. Despite having similar electric structure and κ_L , Li_3Sb has a higher ZT thus an excellent TE performance. Therefore, finally we explain why Li_3Sb has a higher ZT compared to Li_3Bi , despite having similar electric structure and κ_L . All influence factors, including Seebeck coefficient S , electronic conductivity σ and electrical thermal conductivity κ_e are discussed and our results show that S , σ , κ_e and κ_L can not determine the TE performances alone. This suggests that enhancing ZT requires optimizing the adversely interdependent S , σ , κ_e and κ_L as a group. Through this work, we propose that p-type doped Li_3Sb and p-type doped Li_3Bi could be more promising TE application materials.

Acknowledgment

This research was supported by the National Natural Science Foundation of China under Grant No. 11774396 and No. 11704322, Shandong Natural Science Funds for Doctoral Program under Grant No. ZR2017BA017, the National Key Research and Development Program of China under Grant No. 2016YFA0300902, Graduate Innovation Foundation of Yantai University, GIFYTU, No. YDZD1810.

ORCID iDs

Zhenhong Dai  <https://orcid.org/0000-0002-8559-3196>

References

- [1] He J and Tritt T M 2017 *Science* **357** 1369
- [2] Snyder G J and Toberer E S 2008 *Nat. Mater.* **7** 105
- [3] Zhao Y, Dai Z, Zhang C, Lian C, Zeng S, Li G, Meng S and Ni J 2017 *Phys. Rev. B* **95** 014307
- [4] Su X et al 2017 *Adv. Mater.* **29** 1602013
- [5] Bell L E 2008 *Science* **321** 1457
- [6] He J, Girard S N, Kanatzidis M G and Dravid V P 2010 *Adv. Funct. Mater.* **20** 764
- [7] Pei Y, LaLonde A, Iwanaga S and Snyder G J 2011 *Energy Environ. Sci.* **4** 2085
- [8] Heremans J P, Jovovic V, Toberer E S, Saramat A, Kurosaki K, Charoenphakdee A, Yamanaka S and Snyder G J 2008 *Science* **321** 554
- [9] Liu W, Tan X, Yin K, Liu H, Tang X, Shi J, Zhang Q and Uher C 2012 *Phys. Rev. Lett.* **108** 166601
- [10] Vashaee D and Shakouri A 2004 *Phys. Rev. Lett.* **92** 106103
- [11] Zhang Y, Bahk J H, Lee J, Birkel C S, Snedaker M L, Liu D, Zeng H, Moskovits M, Shakouri A and Stucky G D 2014 *Adv. Mater.* **26** 2755
- [12] Lan Y, Minnich A J, Chen G and Ren Z 2010 *Adv. Funct. Mater.* **20** 357
- [13] Vineis C J, Shakouri A, Majumdar A and Kanatzidis M G 2010 *Adv. Mater.* **22** 3970
- [14] Olvera A A, Moroz N A, Sahoo P, Ren P, Bailey T P, Page A A, Uher C and Poudeu P F P 2017 *Energy Environ. Sci.* **10** 1668
- [15] Li W and Mingo N 2014 *Phys. Rev. B* **89** 184304

- [16] Lindsay L and Parker D S 2015 *Phys. Rev. B* **92** 144301
- [17] Li W and Mingo N 2015 *Phys. Rev. B* **91** 144304
- [18] Bayerl D and Kioupakis E 2015 *Phys. Rev. B* **91** 165104
- [19] Hao Q, Xu D, Lu N and Zhao H 2016 *Phys. Rev. B* **93** 205206
- [20] Chan H, Candace K, Peng H, Liu G, McIlwrath K, Zhang X F, Huggins R A and Cui Y 2007 *Nat. Nanotechnol.* **3** 31
- [21] Bruce P, Scrosati B and Tarascon J 2008 *Angew. Chem., Int. Ed. Engl.* **47** 2930
- [22] Pang Q, Liang X, Kwok C Y, Kulisch J and Nazar L F 2017 *Adv. Energy Mater.* **7** 1601630
- [23] Liu Z, Wang Y, Mao J, Geng H, Shuai J, Wang Y, He R, Cai W, Sui J and Ren Z 2016 *Adv. Energy Mater.* **6** 1502269
- [24] Yang X, Zhao Y, Dai Z, Zulfiqar M, Zhu J and Ni J 2017 *Phys. Lett. A* **381** 3514
- [25] Li W, Carrete J, Katcho N A and Mingo N 2014 *Comput. Phys. Commun.* **185** 1747
- [26] Kresse G and Furthmüller J 1996 *Comput. Mater. Sci.* **6** 15
- [27] Togo A, Oba F and Tanaka I 2008 *Phys. Rev. B* **78** 134106
- [28] Kresse G and Joubert D 1999 *Phys. Rev. B* **59** 1758
- [29] Perdew J P, Burke K and Ernzerhof M 1996 *Phys. Rev. Lett.* **77** 3865
- [30] Madsen G K and Singh D J 2006 *Comput. Phys. Commun.* **175** 67
- [31] Sangster J and Pelton A D 1993 *J. Phase Equilib.* **14** 514
- [32] Sangster J and Pelton A D 1991 *J. Phase Equilib.* **12** 447
- [33] Leonova M E, Sevast'yanova L G, Gulish O K and Burdina K P 2001 *Inorg. Mater.* **37** 1270
- [34] Wei S H and Zunger A 1987 *Phys. Rev. B* **35** 3952
- [35] Kalarasse L, Bennecer B and Kalarasse F 2011 *Comput. Mater. Sci.* **50** 2880
- [36] Togo A and Tanaka I 2015 *Scr. Mater.* **108** 1
- [37] Zeeshan M, Singh H K, van den Brink J and Kandpal H C 2017 *Phys. Rev. Mater.* **1** 075407
- [38] Joshi G, Yan X, Wang H, Liu W, Chen G and Ren Z 2011 *Adv. Energy Mater.* **1** 643
- [39] Joshi G et al 2008 *Nano Lett.* **8** 4670
- [40] Fu T, Yue X, Wu H, Fu C, Zhu T, Liu X, Hu L, Ying P, He J and Zhao X 2016 *J. Materiomics* **2** 141
- [41] Tang Y, Gibbs Z M, Agapito L A, Li G, Kim H S, Nardelli M B, Curtarolo S and Snyder G J 2015 *Nat. Mater.* **14** 1223
- [42] Joshi G et al 2014 *Energy Environ. Sci.* **7** 4070